Evidence for Changes in the Nucleotide Conformation in the Active Site of H^+-ATPase As Determined by Pulsed EPR Spectroscopy

Benoît Schneider,[‡,§] Claude Sigalat,[‡] Toyoki Amano,[||] and Jean-Luc Zimmermann*[,‡]

CEA/Saclay, Département de Biologie Cellulaire et Moléculaire, Section de Bioénergétique, Bât. 532, F-91191 Gif-sur-Yvette, France, and Department of Biology and Geosciences, Shizuoka University, Shizuoka 422-8529, Japan

Received June 26, 2000; Revised Manuscript Received October 6, 2000

ABSTRACT: The conformation of di- and triphosphate nucleosides in the active site of ATPsynthase (H^+-ATPase) from thermophilic *Bacillus PS3* (TF1) and their interaction with Mg^{2+}/Mn^{2+} cations have been investigated using EPR, ESEEM, and HYSCORE spectroscopies. For a ternary complex formed by a stoichiometric mixture of TF1, Mn^{2+}, and ADP, the ESEEM and HYSCORE data reveal a ^{31}P hyperfine interaction with Mn^{2+} ($|A(^{31}P)| \approx 5.20$ MHz), significantly larger than that measured for the complex formed by Mn^{2+} and ADP in solution ($|A(^{31}P)| \approx 4.50$ MHz). The *Q*-band EPR spectrum of the Mn·TF1·ADP complex indicates that the Mn^{2+} binds in a slightly distorted environment with $|D| \approx 180 \times 10^{-4}$ cm^{-1} and $|E| \approx 50 \times 10^{-4}$ cm^{-1}. The increased hyperfine coupling with ^{31}P in the presence of TF1 reflects the specific interaction between the central Mn^{2+} and the ADP β-phosphate, illustrating the role of the enzyme active site in positioning the phosphate chain of the substrate for efficient catalysis. Results with the ternary Mn·TF1·ATP and Mn·TF1·AMP−PNP complexes are interpreted in a similar way with two hyperfine couplings being resolved for each complex ($|A(^{31}P_\beta)| \approx 4.60$ MHz and $|A(^{31}P_\gamma)| \approx 5.90$ MHz with ATP, and $|A(^{31}P_\beta)| \approx 4.20$ MHz and $|A(^{31}P_\gamma)| \approx 5.40$ MHz with AMP−PNP). In these complexes, the increased hyperfine coupling with $^{31}P_\gamma$ compared with $^{31}P_\beta$ reflects the smaller Mn···P distance with the γ-phosphate compared with the β-phosphate as found in the crystal structure of the analogous enzyme from mitochondria [3.53 vs 3.70 Å (Abrahams, J. P., Leslie, A. G. W., Lutter, R., and Walker, J. E. (1994) *Nature 370*, 621−628)] and the different binding modes of the two phosphate groups. The ESEEM and HYSCORE data of a complex formed with Mn^{2+}, ATP, and the isolated β subunit show that the ^{31}P hyperfine coupling is close to that measured in the absence of the protein, indicating a poorly structured nucleotide site in the isolated β subunit in the presence of ATP. The inhibition data obtained for TF1 incubated in the presence of Mg^{2+}, ADP, $Al(NO_3)_3$, and NaF indicate the formation of the inhibited complex with the transition state analogue namely Mg·TF1·ADP·AlF_x with the equilibrium dissociation constant $K_D = 350$ μM and rate constant $k = 0.02$ min^{-1}. The ESEEM and HYSCORE data obtained for an inhibited TF1 sample, Mn·TF1·ADP·AlF_x, confirm the formation of the transition state analogue with distinct spectroscopic footprints that can be assigned to Mn···^{19}F and Mn···^{27}Al hyperfine interactions. The $^{31}P_\beta$ hyperfine coupling that is measured in the inhibited complex with the transition state analogue ($|A(^{31}P_\beta)| \approx 5.10$ MHz) is intermediate between those measured in the presence of ADP and ATP and suggests an increase in the bond between Mn and the P_β from ADP upon formation of the transition state.

F-type H^+-ATPsynthases are metabolic enzymes that catalyze the reversible phosphorylation of adenosine diphosphate (ADP)[1] to adenosine triphosphate (ATP) by using a transmembrane proton gradient as a source of energy. F-type H^+-ATPsynthases have been isolated, purified, and some have been cloned from several prokaryotic organisms and eukaryotic organelles such as *Escherichia coli*, *Bacillus PS3*, mitochondria, and chloroplasts (for a review, see ref *1*). The enzyme complex consists of a large number of subunits of which the amino acid sequences are highly conserved among different species. F-type H^+-ATPsynthases are composed of two distinct parts. F0, the membrane-spanning part, mediates proton transport to F1, the extrinsic part of the enzyme which catalyzes the phosphorylation reaction. The soluble F1 part that can be isolated from the complex is an ATPase enzyme that only retains the ability to hydrolyze ATP to ADP.

* To whom correspondence should be addressed. Phone: +33 (0) 169 08 68 39. Fax: +33 (0) 169 08 87 17. E-mail: jean-luc.zimmermann@cea.fr.

‡ CEA/Saclay.

§ Present address: Institut Pasteur, Unité de Régulation Enzymatique des Activités Cellulaires, 25, rue du Docteur Roux, 75724 Paris cedex 15, France.

|| Department of Biology and Geosciences.

[1] Abbreviations: ADP, adenosine 5′-diphosphate; AlF_x, a fluoroaluminate anion, AlF_3 or AlF_4^-; AMP−PNP, adenosine 5′-(β,γ-imido)-triphosphate; ATP, adenosine 5′-triphosphate; AXP, an adenosine nucleotide; DCCD, dicyclohexyl-carbodiimide; EDTA, ethylenediaminetetraacetic acid; EPR, electron paramagnetic resonance or, equivalently, electron spin resonance or ESR; ESEEM, electron spin−echo envelope modulation; FT, Fourier transform; GAP, GTP activating protein; HYSCORE, hyperfine sublevel correlation spectroscopy; MF1, F1 H^+-ATPase from bovine heart mitochondria; NBD-Cl, 7-chloro-4-nitrobenzo-2-oxa-1,3-diazole; TF1, F1 H^+-ATPase from thermophilic *Bacillus* PS3.

10.1021/bi0014599 CCC: $19.00
Published on Web 11/21/2000

The X-ray structures of the F1 part of the bovine mitochondrial enzyme (MF1) and of the $\alpha_3\beta_3$ crown of the thermophilic *Bacillus* PS3 enzyme (TF1) have been determined at high resolution (*2*, *3*). Comparison of the two published structures shows that the overall folding of each subunit and the structure of the active site are both remarkably conserved. The F1 part of F-type H^+-ATPsynthases is composed of five different protein subunits ($\alpha_3\beta_3\gamma\delta\epsilon$) and bears six nucleotide binding sites (*4*−*6*). Three of these sites are catalytic and are believed to be directly involved in the phosphorylation reaction, whereas the three other sites are non catalytic with much less clear function (*7*). By chemical inactivation with reagents such as DCCD and NBD-Cl, and photoaffinity-labeling experiments with nucleotide analogues, it has been demonstrated that the catalytic sites are mainly located on the β subunits but also involve some residues from the α subunits which may interact with the nucleotide (*8*). Among the residues located at the active site, it was shown based on mutagenesis data that β-Tyr340 is involved in stacking the adenine ring of the nucleotide and provides a nonpolar environment.[2] The ribose does not appear to make any specific interaction with the protein. Residues from the β subunits and belonging to the conserved motif known as the P-loop (GGAGVGKT) enfold the phosphate moieties in the nucleotide binding sites: β-Lys-164 and β-Thr165 appear to have a direct function in nucleotide binding and catalysis by, respectively, H-bonding the γ-phosphate of the nucleotide and providing a coordination ligand to the Mg^{2+} ion cofactor (*2*, *9*).

The catalytic mechanism of ATP hydrolysis has been completely described in kinetic and thermodynamic terms by studying the unisite reaction that involves a single catalytic site (*1*). The actual chemical reaction of ATP hydrolysis is generally assumed to proceed by an in-line nucleophilic attack of a water molecule on the terminal γ-phosphate, following an associative mechanism and involving a pentacovalent phosphorus transition state (*10*). The ATP synthesis reaction seems to proceed with inversion of the configuration of the oxygen atoms about the terminal phosphorus, with ADP−O being the acceptor for Pi, and no phosphoenzyme intermediate (*11*, *12*). In fact, the involvement of active site protein residues in these chemical mechanisms and possible conformational changes of the catalytic site are largely unknown. However, the catalytic pathway is outlined by the information available from the X-ray structures of MF1 with dead-end complexes with AMP−PNP and ADP (*2*) and of the TF1 $\alpha_3\beta_3$ subcomplex (*3*). Due to the turnover of the enzyme, natural triphosphate nucleosides such as ATP are not suitable for the crystallographic characterization of nucleotidases with hydrolysis intermediates. Instead, aluminum fluorides (AlF_3 or AlF_4^-) in the presence of diphosphate nucleosides, appear to mimic the transition state for a number of nucleotidases, including the Gα protein (*13*), actin and tubulin (*14*, *15*), the F_1-ATPase from mitochondria (*16*), the p21 *ras* complex with GAP (*17*), and nucleoside diphosphate kinase (*18*). In particular, it has been reported that full inactivation of MF1 is accompanied by the formation of two moles of an ADP fluorometal complex per mole of enzyme (*16*). By contrast, the formation of an ADP fluoroaluminate complex at a single catalytic site was shown to be sufficient for complete inactivation of the wild-type $\alpha_3\beta_3\gamma$ subcomplex of TF1 (*19*). In these studies, the presence of Mg^{2+} cations was shown to be necessary for the formation of the ADP fluorometal complex.

The Mg^{2+} cation acts as an essential cofactor for both the ATP synthesis and hydrolysis reactions of F1 (*20*). The presence of Mg^{2+} has also been reported to convey high-affinity binding cooperativity in F1 (*21*, *22*). Among the other divalent metal cations that may replace the natural Mg^{2+} in the hydrolysis reaction, Mn^{2+} is of special interest because its paramagnetic properties as detected by EPR and ESEEM can be used to study both its binding site in F1 and its interaction with the nucleotides (*23*, *24*). In the latter study, it was shown that the TF1 enzyme can be completely depleted of its natural Mg^{2+}, and that complexes of Mn^{2+} with TF1 could be generated that showed specific EPR properties. In the absence of nucleotide, TF1 binds Mn^{2+} with a nitrogen ligand that was proposed to arise from β-Lys164. In the presence of ATP, coordination of the Mn^{2+} by the phosphate moieties of the nucleotide was also inferred from the ESEEM spectra (*24*).

In the present study, we have extended this investigation on the nucleotide binding sites of TF1, by studying the EPR properties of Mn^{2+} bound to a catalytic site in the presence or absence of nucleotides. In addition to detecting the nuclear frequencies associated with the protein and nucleotide ligands to the Mn^{2+} by the ESEEM technique of pulsed EPR, we report a series of two-dimensional HYSCORE spectra of Mn^{2+} bound to TF1 in complexes with ADP, ATP, and the inhibitor AMP−PNP that show evidence for couplings between the Mn^{2+} and the ^{31}P nuclei from the nucleotide phosphates. Interestingly, substantial differences in the ^{31}P hyperfine couplings that depend on the bound nucleotide can be measured by this method, and these can be related to the differences in the coordination of Mn^{2+} with the nucleotides bound to TF1. The interaction of ATP with the isolated β subunit of TF1 was also examined by ESEEM and HYSCORE. The spectroscopic data are similar to those in the absence of the protein, suggesting a poorly structured nucleotide site in the isolated β subunit.

In addition to the ternary TF1 complexes with Mn^{2+} and the nucleotide substrate (ATP), the substrate analogue (AMP−PNP) or the product (ADP), a complex of TF1 with Mn^{2+} and a transition state analogue of the ATP hydrolysis reaction has been examined by ESEEM and HYSCORE. This experiment was performed by using fluoroaluminate as an analogue of inorganic phosphate bound at the active site. The formation of the transition state analogue under the unisite conditions used for the EPR measurements was inferred from enzymatic results that indicate complete and irreversible inhibition of TF1 under the conditions used. The ESEEM spectra show that the Mn^{2+} bound at a catalytic site is coupled to ^{19}F ($I = {}^1/_2$) and ^{27}Al ($I = {}^5/_2$) atoms from AlF_x, demonstrating the proximity of the Mn^{2+} and AlF_x moieties. Coordination of the Mn^{2+} by the phosphate appears to have properties that are similar to those measured when ADP or ATP are bound at the catalytic site. These results are discussed with respect to the mechanism proposed for ATP hydrolysis derived from kinetic measurements of MF1 from rat liver in the presence of orthovanadate, which has recently been studied as another transition state mimic (*25*).

[2] Except otherwise stated, the amino acid numbering refers to the sequences of the *Bacillus* PS3 enzyme subunits.

MATERIALS AND METHODS

Materials. ATP (disodium salt), ADP (monopotassium salt), AMP−PNP (tetralithium salt), lactate dehydrogenase, and pyruvate kinase were from Boehringer Mannheim. $MnCl_2$, $Al(NO_3)_3$, NaF, NADH, and phosphoenol pyruvate (PEP) were from Sigma.

Purification of TF1 and Preparation of the β Subunit. H^+-ATPase from thermophilic *Bacillus* PS3 (TF1) was extracted from cells that were grown at the Laboratoire d'Extraction (CNRS, Gif-sur-Yvette, France). The cell paste was stored at −80 °C until use. The extraction and purification of TF1 was performed as described previously (*24*), and the protein was stored at 4 °C as a precipitate in ammonium sulfate at 34%. For preparation of the EPR samples, the enzyme precipitate was dialyzed for 24 h against 50 mM HEPES−KOH and 10 mM EDTA at pH 8.0 in order to remove all nucleotides and divalent metal cations bound to the enzyme. This dialysis step was followed by a second 48 h dialysis against 50 mM HEPES−KOH at pH 8.0. When necessary the protein was concentrated to ∼50 mg/mL for the purpose of EPR measurements. Protein concentration was determined using $\epsilon_{280} = 0.455$ cm^2 mg^{-1} for TF1 (*26*). The enzyme was pure at 99% as judged by SDS−PAGE. The molecular weight of the protein was taken as 385 350 (*27*).

The Mg^{2+} content of TF1 was determined by atomic absorption spectroscopy as previously described (*24*). The absence of nucleotides in TF1, in particular of the strongly bound nucleotide that is found in the analogous chloroplast enzyme CF1, was verified a posteriori from the absence of the characteristic ^{31}P peaks in the ESEEM of the enzyme complex with Mn^{2+}.

The β subunit of TF1 expressed in *Escherichia coli* strain DK8 was purified as described previously (*28*).

Activity Measurements. Inhibition studies of TF1 by fluoroaluminates were performed in the following way: the enzyme (3.3 μM) was incubated at 60 °C in 50 mM HEPES−KOH, pH 8.0, in the presence of ADP (3.3 μM), $Al(NO_3)_3$ (200 μM), NaF (5 mM), and various amounts of $MgCl_2$ (see legend to Figure 9). Aliquots of 5 μL were withdrawn after increasing times of incubation and the residual ATPase activity was determined spectrophotometrically at 37 °C by following the absorbance change of NADH at 340 nm with the regenerating system previously described (*29*) except that the ATP concentration was 1 mM. As observed previously, the hydrolysis rate by TF1 initially displays a short lag which accelerates to a final constant rate within 2 min. This final hydrolysis rate V is directly proportional to the amount of noninhibited enzyme. The kinetics of inhibition were all found to follow a monoexponential progress, and the rate constants for inactivation were calculated from semilogarithmic plots of V/V_0 versus time, where V_0 is the rate at incubation time $t = 0$, i.e., just after mixing TF1 with ADP, $Al(NO_3)_3$, NaF, and $MgCl_2$.

EPR sample preparation. For all EPR experiments, $MnCl_2$ and/or nucleotides were added from millimolar solutions in 50 mM HEPES−KOH, pH 8.0, to the metal-depleted protein samples in stoichiometric conditions. The EPR samples were immediately frozen and stored in liquid N_2 until the EPR measurements were performed.

The EPR sample with TF1 inhibited with fluoroaluminates was made with EDTA-treated TF1 (50 μM) incubated with $MnCl_2$ (50 μM), ADP (50 μM), $Al(NO_3)_3$ (3 mM), and NaF (75 mM) in 50 mM HEPES−KOH, pH 8.0, at 60 °C. After a 6 h incubation period, the residual activity was 1%, and the EPR sample was immediately frozen in liquid N_2.

EPR Measurements. EPR spectra at Q-band were recorded with a Bruker ER 200D spectrometer equipped with a cylindrical cavity (ER 4910). The spectra were recorded at ∼240 K using a liquid N_2 cryostat. Spectral simulations were performed as described previously (*24*) using the algorithm reported in (*30*, *31*). Pulsed ESEEM experiments were all carried out at 4.2 K using a Bruker ER380 pulsed EPR spectrometer operating at X-band. The two-pulse ESEEM spectrum was obtained by measuring the magnetization echo produced by the $\pi/2-\tau-\pi$ pulse sequence as a function of time τ. τ was typically incremented from 112 to 6400 ns by 8 ns steps. The three-pulse sequence uses three $\pi/2$ pulses and produces a stimulated echo. The amplitude of the echo is digitized as a function of $\tau + T$, where τ is the time separating the first two pulses and T the time between the second and the third pulses. In this experiment, time τ is fixed, and time T is incremented from 80 to 6320 ns. The τ values were generally chosen close to twice the proton Larmor period (67.1 ns at 350 mT) to induce the suppression effect for this frequency that otherwise dominates the three-pulse ESEEM spectrum. The phase cycling algorithm reported in ref *32* was used to eliminate the contribution of secondary echoes to the three-pulse ESEEM signal. The signal was then processed for deadtime correction and Fourier transformation as described previously (*24*) to yield the three-pulse ESEEM spectrum in the frequency domain.

2D HYSCORE spectra were obtained using the 4-pulse sequence $\pi/2-\tau-\pi/2-t_1-\pi-t_2-\pi/2$ described previously (*33*). Ideally, the stimulated echo produced by the three $\pi/2$ pulses of the sequence is completely inverted by the π pulse. Experimentally, the length and power of the π pulse were adjusted to optimize this inversion, to minimize the on-diagonal features in the FT (*34*, *35*). The amplitude of the inverted echo was recorded as a function of the two characteristic times t_1 and t_2. The 200 × 200 data array was processed and Fourier transformed as described previously (*36*) using the Bruker WinEPR software. The results in this paper are presented as contour plots obtained after Fourier transformation and magnitude calculation. These appear in two quadrants referred to as the positive and negative quadrants. The f_1 and f_2 frequency axes of these quadrants correspond to the times t_1 and t_2 of the pulse sequence.

RESULTS

Interaction between TF1 and ADP, ATP, and AMP−PNP. Figure 1 shows a series of three-pulse ESEEM spectra measured for TF1 at 345.4 mT. The spectra were obtained for TF1 depleted of its nucleotides and metal cations after the treatment with EDTA (see Materials and Methods) and subsequently replenished with a stoichiometric amount of Mn^{2+} (i.e., 1 mol of Mn^{2+}/mol of enzyme). The spectrum in Figure 1A was obtained for a sample with no added nucleotide while those in panels B−D of Figure 1 were obtained in the presence of ADP, ATP, and AMP−PNP (1 mol of nucleotide/mol of enzyme), respectively. The ESEEM spectra measured in this manner display frequencies that

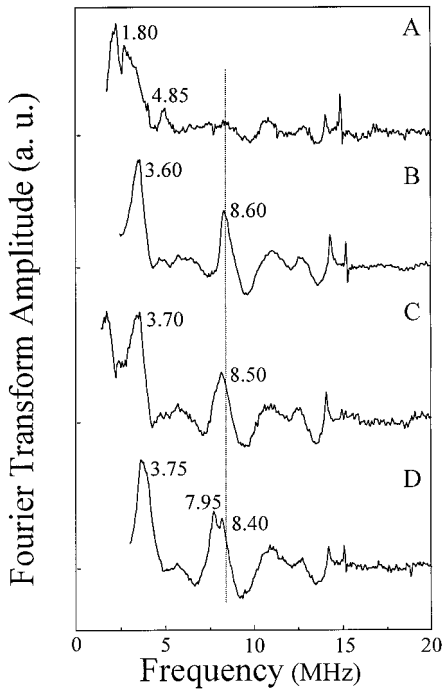

FIGURE 1: Three-pulse Fourier transform ESEEM spectra of Mn^{2+} bound to TF1 with no further additions (A), with added ADP (B), with added ATP (C) or with added AMP−PNP (D) under stoichiometric conditions. Samples were frozen immediately after addition of Mn^{2+} and nucleotide to the enzyme solution. The data were obtained at a temperature of 4.2 K, a microwave frequency f = 9.63 GHz, and a magnetic field setting H = 345.4 mT. The interpulse time τ was 136 ns and the time interval between successive spin−echo pulse sets was 2 ms. The sharp feature at 15.6 MHz is a submultiple of the Nyquist frequency and is a sampling artifact.

correspond to the different magnetic couplings experienced by the Mn^{2+} cation in the sample. These couplings originate from nuclei with nonzero magnetic moments such as ^1H, ^{14}N, or ^{31}P that are located in the vicinity of the Mn^{2+} paramagnet. All four spectra in Figure 1 show a small peak at 14.7 MHz, the H^+ Larmor frequency, that is not completely suppressed by the choice of τ = 136 ns. This peak arises from neighboring hydrogen atoms that are dipolar coupled to the Mn^{2+} ion. Since our interest will be mostly focused on the protein and nucleotide ligands of the Mn^{2+}, this frequency component will not be further discussed. The spectrum in Figure 1A obtained for TF1 with 1 Mn^{2+} and no added nucleotide is characterized by a series of low (<5 MHz) frequency components and is essentially identical to the spectrum that was already reported for this kind of preparation (*24*). On the basis of the crystal structure that is available for MF1, this was proposed to correspond to the coordination of Mn^{2+} by the ϵ-amine group of β-Lys-164 in TF1 in the absence of nucleotide. Of particular note in Figure 1A is the absence of frequencies attributable to coupling of Mn^{2+} with ^{31}P, confirming the total depletion of nucleotide from TF1 by the EDTA treatment. The spectrum in Figure 1B is obtained when both Mn^{2+} and ADP are added in stoichiometric amounts to the TF1 sample. Here the ESEEM spectrum is different, demonstrating a change in the coordination of the Mn^{2+} cation when the nucleotide is added. Two frequencies dominate the spectrum at 3.60 and 8.60 MHz. A less intense feature that appears as a negative peak at ~12.4 MHz is also a reproducible feature in the spectrum.

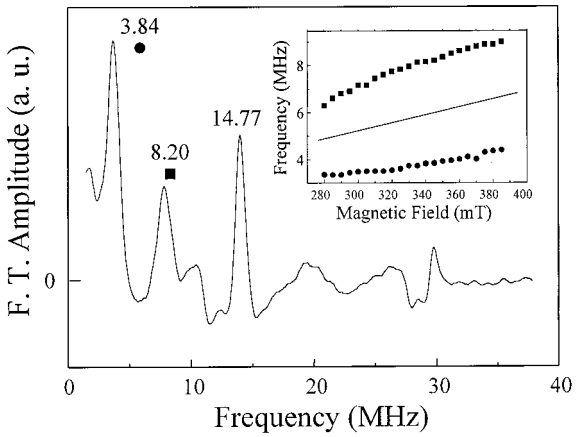

FIGURE 2: Two-pulse Fourier transform ESEEM spectrum of the Mn^{2+} complex formed with $MnCl_2$ 9.5 mM and ATP 20 mM, pH 8.2, in a H_2O/glycerol 50/50 mixture. The data were obtained at a temperature of 4.2 K, a microwave frequency f = 9.66 GHz, and a magnetic field setting of 345.0 mT. The time interval between successive spin−echo pulse sets was 1.64 ms. The inset shows the dependence of the observed ^{31}P frequencies as the external magnetic field is changed between 280.0 and 385.0 mT.

Similar patterns of frequency components are found for the samples with ATP (Figure 1C) and AMP−PNP (Figure 1D), thereby suggesting that they probably correspond to some interaction between the Mn^{2+} ion and the nucleotide. It is of particular note that differences in terms of the position, the width or the splitting of the peak at ~8.5 MHz can be measured for the three different samples, that may correspond to different interactions between the Mn^{2+} and ADP, ATP, or AMP−PNP.

The two major peaks at 3.60 and 8.60 MHz in the spectrum of the TF1 sample with ADP (Figure 1B) are disposed about the free ^{31}P Larmor frequency ν_L = 5.96 MHz. The two peaks form a nearly symmetrical pattern similar to that reported for other Mn^{2+}-nucleotide systems (*24*, *37-42*). The pattern is also analogous to that observed in the two-pulse ESEEM spectrum measured in (*37*) for a control sample containing Mn^{2+} (9.5 mM) and ATP (20 mM) (Figure 2). In this latter spectrum, the two peaks at 3.84 and 8.20 MHz correspond to the coupling with the ^{31}P of the phosphate ligands of the ATP. Similarly, the two peaks in the spectra of Figure 1, panels B−D, for the complexes formed with Mn^{2+} in the presence of TF1 and nucleotide are attributed to the coupling that involves the central $M_S = \pm 1/2$ EPR transition of Mn^{2+} and ^{31}P ($I = 1/2$) from a phosphate ligand of the nucleotide. An isotropic hyperfine coupling of about 5 MHz can be estimated from the frequency separation of the two ESEEM peaks. As a support for the assignment of the ESEEM peaks to ^{31}P nuclear frequencies, the spectra were also collected at different magnetic field settings within the Mn^{2+} EPR absorption line. In this manner, the field dependence of the ESEEM peaks is obtained by tracking the positions of the peaks in the ESEEM spectra as the magnetic field is changed (see inset to Figure 2). In the central portion of the studied range, between ~320 mT and ~370 mT, the two ESEEM frequencies closely follow the magnetic field dependence of the ^{31}P Larmor frequency (Figure 2, inset, straight line). This reflects the fact that the two peaks arise from the coupling of ^{31}P ($I = 1/2$) with the central $M_S = \pm 1/2$ transition of Mn^{2+}. Particularly at low fields and, to a lesser extent, at high fields,

the linear relationship is broken and the dependence displays a marked curvature that reflects the contribution of the two neighboring $-3/2 \leftrightarrow -1/2$ and $+1/2 \leftrightarrow +3/2$ fine structure transitions to the coupling (*41*). The magnetic field dependence of the ESEEM peaks from ^{31}P coupled to Mn^{2+} therefore reflects the high spin multiplicity of Mn^{2+} ($S = 5/2$). This has also been reported for other Mn^{2+} systems with nucleotides and has been best studied by Singel and co-workers (*41*). The ESEEM peaks at ~3.6 and ~8.5 MHz in the enzyme containing samples were found to display a very similar magnetic field dependence (not shown). Therefore, it is concluded that they correspond to coupling between the Mn^{2+} ion and the ^{31}P from the nucleotide.

The ESEEM spectra in Figure 1, panels B−D, were obtained with samples for which equimolar amounts of TF1, Mn^{2+}, and nucleotide were added together. As mentioned above, the spectra are evidence for coupling of the Mn^{2+} with the phosphate groups of the nucleotides, and the magnitude of the hyperfine coupling demonstrates the coordination of the Mn^{2+} ion by the nucleotide phosphate(s). Since there is no specific signature from TF1 in these spectra, there is no direct indication that the protein does indeed intervene in some way in the positioning of the Mn^{2+} ion or the nucleotide and that the spectra actually represent Mn^{2+} bound to TF1. A number of points are relevant to this question. First, it is of note that the nucleotide binding site with the highest affinity in F1 has a $K_D = 0.2-0.4$ nM (*43*, *44*). This indicates that with the concentrations used in the present study (TF1, AXP, and Mn^{2+}, 100 μM), the ternary complexes Mn·TF1·ADP, Mn·TF1·ATP, and Mn·TF1·AMP−PNP are the predominant forms at >97% in solution. The spectra that are shown in Figure 1 are therefore representative of the different Mn^{2+}·AXP complexes bound to TF1. Second, the Q-band EPR spectra recorded for all the enzyme samples display the characteristic features arising from the effect of zero-field splitting (forbidden transitions, line splittings at high field) on the Mn^{2+} energy levels. A representative spectrum is that obtained for the Mn^{2+}·TF1·ADP sample (Figure 3). The modest but significant zero-field splitting ($|D| \approx 180 \times 10^{-4}$ cm^{-1} and $|E| \approx 50 \times 10^{-4}$ cm^{-1} calculated from spectral simulation) contrasts with the absence of zero-field splitting when the enzyme is omitted from the sample (not shown). And last, the three-pulse ESEEM spectra were also recorded for samples made using the same procedure and concentrations as in Figure 1, except that TF1 was omitted from the samples (Figure 4). These spectra are clearly different from those in Figure 1. More specifically, the sample with Mn^{2+} and ADP displays a broad peak that can be assigned to coupling with a ^{31}P from ADP, but the frequency position is different at 8.20 MHz compared with 8.60 MHz in the presence of TF1, indicating that the hyperfine coupling is smaller in the absence of the protein. The sample with the Mn·ATP complex shows a very similar spectrum (Figure 4B), indicating that, in the absence of the enzyme, the nature of the nucleotide does not really influence the ^{31}P hyperfine interaction. Here again, the observed ^{31}P frequency at 8.20 MHz is clearly different from that at 8.50 MHz observed in the presence of TF1. Consequently, it is concluded that the ESEEM spectra in Figure 1, panels B−D, indeed reflect the environment of Mn^{2+} bound to TF1.

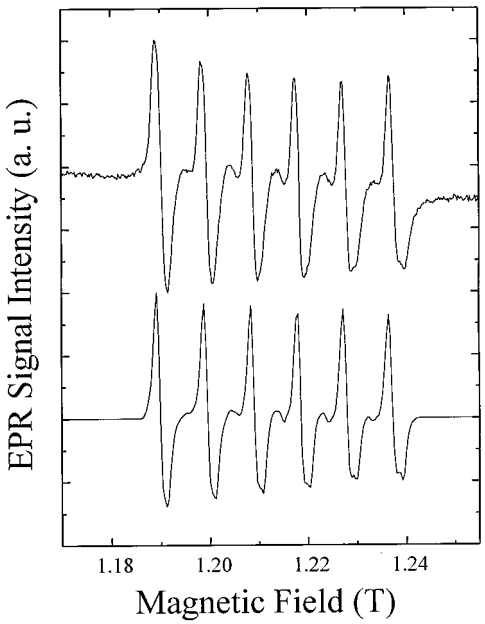

FIGURE 3: Q-band EPR spectrum measured for the Mn·TF1·ADP sample (top) and its simulation (bottom). The experimental conditions were: temperature, 236 K; microwave power, 2 mW; modulation amplitude, 0.5 mT; microwave frequency, 33.99 GHz. The simulated spectrum was calculated using $g_{iso} = 2.0$, $A_{iso} = 88.25 \times 10^{-4}$ cm^{-1}, $|D| = 180 \times 10^{-4}$ cm^{-1}, $|E| = 50 \times 10^{-4}$ cm^{-1}, and a line width of 0.7 mT.

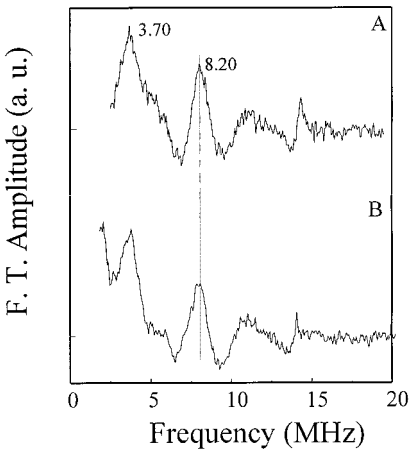

FIGURE 4: Three-pulse Fourier transform ESEEM spectra of frozen solutions of Mn^{2+} complexed with ADP (A) and ATP (B) under stoichiometric conditions. Experimental conditions were the same as in Figure 1.

Close inspection of the spectra in Figure 1 shows that the ^{31}P peak at 8.50 MHz in the ATP sample (Figure 1C) is significantly broader than the corresponding peak at 8.60 MHz in the ADP sample (Figure 1B), suggesting that the former may in fact encompass unresolved features. In addition, Figure 1D shows that with AMP−PNP, two peaks are indeed resolved at 7.95 and 8.40 MHz, suggesting that the Mn^{2+} experiences two ^{31}P couplings of different magnitudes. To further characterize the couplings revealed by the three-pulse ESEEM spectra, and to possibly delineate frequency components that may superimpose in the one-dimensional spectra of Figure 1, 2D HYSCORE spectra were recorded. In these spectra, useful information can be extracted from correlation peaks that appear as mirror components on each side of the diagonals of the positive (f_1, f_2) and negative

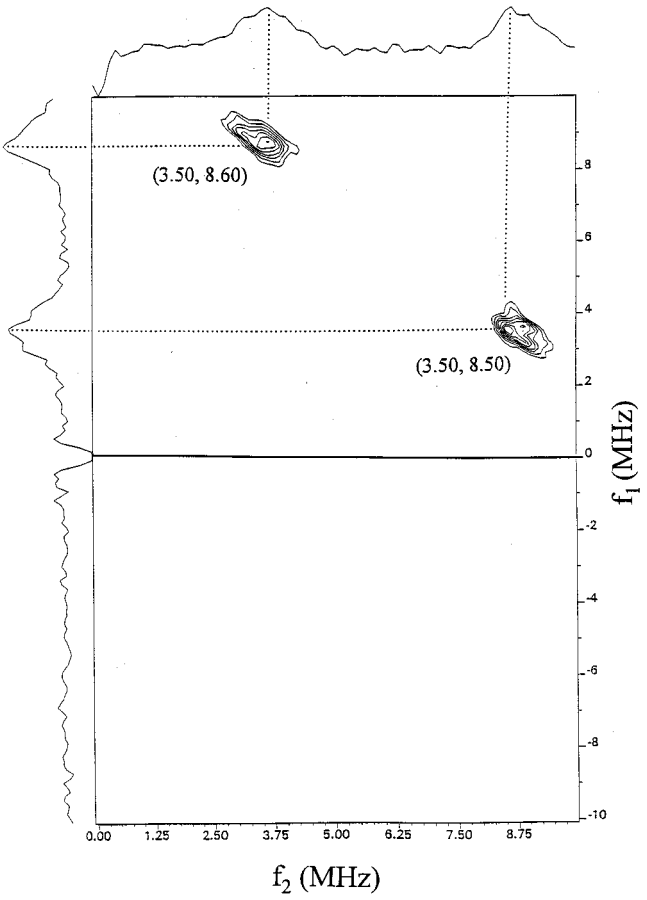

FIGURE 5: HYSCORE contour plot (positive and negative quadrants) of Mn^{2+} in the presence of TF1 (1 Mn/TF1) and ADP (1 ADP/TF1). The data were recorded at $T = 4.2$ K, with a microwave frequency $f = 9.62$ GHz, time $\tau = 168$ ns and magnetic field H = 345.4 mT. The initial t_1 and t_2 were 80 ns and the time increments $\Delta t_1 = \Delta t_2 = 16$ ns. The dotted lines highlight the frequency coordinates of the correlation peaks.

(f_1, $-f_2$) quadrants (*33*). For systems with $S = {}^1/_2$ and $I = {}^1/_2$, the positions and shapes of the correlation peaks observed in the two quadrants may be used to extract the components of the hyperfine interaction (*45*). When $S = {}^1/_2$ and $I = 1$, a situation encountered for the coupling with a ^{14}N nucleus, correlation peaks may be detected between the two $\Delta M_I = 2$ nuclear transitions of the nitrogen (*36*, *46*, *47*). The situation is much less characterized for systems with $S = {}^5/_2$ which is the case for Mn^{2+}. However, the spectra shown in Figures 5−7 for the ternary complexes Mn·TF1·ADP, Mn·TF1·ATP and Mn·TF1·AMP−PNP do show off diagonal features that are symmetrically disposed on each side of the diagonal of the positive quadrant. For the Mn·TF1·ADP sample, the frequencies of the features in the 2D HYSCORE contour correspond to the frequencies in the 1D ESEEM spectra: the two correlations at ∼(3.50, 8.55) MHz (Figure 5) clearly refer to the two ESEEM frequencies at 3.60 and 8.60 MHz (Figure 1B). The correlation pair is therefore assigned to coupling with a ^{31}P from the ADP. Since it was shown that the two ESEEM peaks mainly correspond to coupling with the $M_S = \pm{}^1/_2$ central transition of the Mn^{2+} (*41*), the HYSCORE correlations observed for the Mn·TF1·ADP complex in Figure 5 are also assigned to the ^{31}P hyperfine coupling with this transition. No other correlation was observed for the Mn·TF1·ADP complex, and for all three complexes examined here, no feature was detected in the negative quadrant (Figure 5).

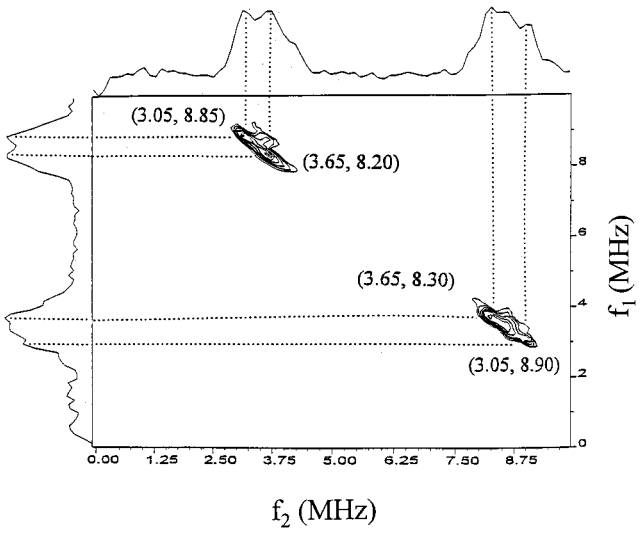

FIGURE 6: HYSCORE contour plot (positive quadrant) of Mn^{2+} in the presence of TF1 (1 Mn/TF1) and ATP (1 ATP/TF1). The experimental conditions were the same as in Figure 5 except $f =$ 9.63 GHz.

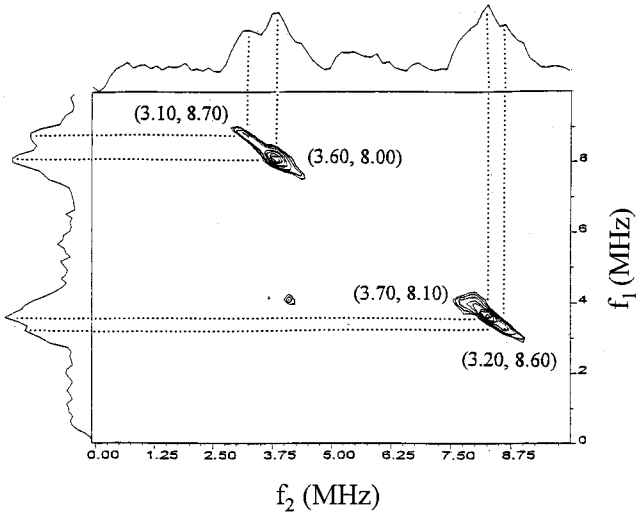

FIGURE 7: HYSCORE contour plot (positive quadrant) of Mn^{2+} in the presence of TF1 (1 Mn/TF1) and AMPPNP (1 AMPPNP/TF1). The experimental conditions were the same as in Figure 5 except for $f = 9.65$ GHz and $\tau = 192$ ns.

The HYSCORE spectra for the samples of the ternary complexes with ATP (Figure 6) and AMP−PNP (Figure 7) show analogous features that are also assigned to couplings with ^{31}P atoms from phosphate ligands. The two spectra also present a significant difference; namely, the shape of the correlation features is more elongated than for the sample with ADP. In fact, this oblong shape results from the presence of two pairs of correlations in each spectrum. These appear as features with twinned peaks in the HYSCORE (Figures 6 and 7). This strongly suggests that in the Mn·TF1·ATP and Mn·TF1·AMP−PNP samples, the Mn^{2+} cation experiences two different ^{31}P couplings that correspond to two different phosphate ligands from the nucleotide triphosphate chain.

When $S = {}^1/_2$ and $I = {}^1/_2$ and in the case of weak hyperfine anisotropy, the two correlation features in the HYSCORE contour are disposed symmetrically about the diagonal and

Table 1: ^{31}P ESEEM Frequencies and Hyperfine Couplings Measured in Mn^{2+} Complexes

sample	^{31}P frequencies at 354.4 mT (MHz)	$\|A(^{31}P)\|$ (MHz)	assignment	d(Mg···P) (Å)[a]	anisotropic factor F (MHz)	isotropic part a (MHz)
Mn·ADP	3.70	4.50	$^{31}P_\beta$ ($^{31}P_\alpha$)			
	8.20					
Mn·ATP	3.70	4.50	$^{31}P_\beta$ and $^{31}P_\gamma$			
	8.20					
Mn·TF1·ADP	3.50	5.20	$^{31}P_\beta$	3.607	0.68	3.84
	8.55					
Mn·TF1·ATP	3.65	4.60	$^{31}P_\beta$			
	8.25					
	3.05	5.90	$^{31}P_\gamma$			
	8.90					
Mn·TF1·AMP−PNP	3.65	4.20	$^{31}P_\beta$	3.699	0.63	2.94
	8.05					
	3.15	5.40	$^{31}P_\gamma$	3.529	0.73	3.94
	8.65					

[a] The distances d(Mg···P) were calculated from the crystal structure of MF1 (Brookhaven Protein Data Bank file 1bmf).

a line joining the two features crosses the diagonal at the (ν_L, ν_L) point where ν_L is the Larmor frequency of the $I = {}^1/_2$ nucleus (here $\nu_L = 5.96$ MHz for ^{31}P). The coordinates ν_1 and ν_2 of the correlations are given by (*48*):

$$\nu_{1,2} = |\nu_L \pm \frac{1}{2}A| \qquad \text{eq 1}$$

where A is, in a first approximation, the average hyperfine coupling, which is close to the isotropic part of the hyperfine coupling. Thus, the hyperfine coupling $|A|$ can be estimated from the separation of the two correlation features in the HYSCORE spectrum. For Mn^{2+} which is the case of interest in the present study, $S = {}^5/_2$, and the above equation does not strictly apply. However, it has been shown for the Mn·TF1·ADP sample that the correlations observed in the Mn^{2+} HYSCORE closely match the frequencies observed in the 1D ESEEM, indicating that the frequency positions of the HYSCORE features may also be defined at first order by eq 1. This may, as already mentioned, result from the fact that the ESEEM frequencies observed for the Mn^{2+} couplings mainly arise from couplings with the central $M_S = \pm{}^1/_2$ transition (*41*). Consequently, eq 1 was also used to obtain a measure of the isotropic hyperfine interaction $|A(^{31}P)|$ between Mn^{2+} and the ^{31}P atoms. Table 1 summarizes these results for the three Mn^{2+} complexes studied here (Mn·TF1·ADP, Mn·TF1·ATP, and Mn·TF1·AMP−PNP) as well as for the control Mn·ADP and Mn·ATP samples. Several points are relevant to the interpretation of the data as given in Table 1. First, it has been shown that the ^{31}P ESEEM frequency in the ~3 MHz region, ν_1, reflects the coupling with small but significant contributions from spin manifolds other than the central $M_S = \pm{}^1/_2$ transition, whereas the other ^{31}P frequency in the ≈8 MHz region, ν_2, has a behavior very close to that expected for a pure $S = {}^1/_2$ system (*41*). Therefore, only ν_2 has been considered in calculating the ^{31}P hyperfine coupling $|A|$, using $|A| = 2 \times |\nu_2 - \nu_L|$. Second, for all the complexes reported in Table 1, the magnitude of the hyperfine couplings with ^{31}P is quite large (4.50−5.90 MHz), indicating that the corresponding phosphate(s) groups(s) coordinate the Mn^{2+}. For the Mn·ATP solution complex, the calculated hyperfine coupling $|A| =$ 4.50 MHz is assigned to $^{31}P_\beta$ and $^{31}P_\gamma$, from the two terminal phosphate groups that coordinate the Mn^{2+}. For the analogous Mn·ADP control sample, the identical hyperfine coupling $|A| = 4.50$ MHz is assigned to the ^{31}P of the coordinating phosphate, i.e., $^{31}P_\beta$. It is also possible that $^{31}P_\alpha$ contributes to the hyperfine coupling if a bidentate Mn^{2+} coordination complex forms with ADP. The ^{31}P hyperfine couplings measured for the samples in the presence of TF1 are interpreted with the help of the X-ray crystallographic data available for MF1, the homologous mitochondrial enzyme filled with nucleotide sites containing ADP and AMP−PNP in the presence of Mg^{2+}. The crystal structure shows that the metal ions are coordinated with the β-phosphate of ADP, and the β- and γ-phosphates of AMP−PNP (*2*). Therefore, it is concluded that the unique ^{31}P hyperfine coupling $|A| \approx$ 5.20 MHz for the Mn·TF1·ADP complex corresponds to $^{31}P_\beta$, whereas the two couplings $|A| \approx 4.20$ MHz and $|A| \approx 5.40$ MHz for Mn·TF1·AMP−PNP correspond to $^{31}P_\beta$ and $^{31}P_\gamma$. By analogy, the ^{31}P couplings at $|A| \approx 4.60$ MHz and $|A| \approx$ 5.90 MHz for the Mn·TF1·ATP complex are attributed to the $^{31}P_\beta$ and $^{31}P_\gamma$.

Because of both the relatively large magnetic moment of the ^{31}P nucleus ($g_N = 2.2632$) and the relatively short Mn···P distances which are expected in the systems under study, the ^{31}P hyperfine couplings reported above may include a significant anisotropic part. In fact, this anisotropic portion can be estimated using a point dipole model with the Mg···P distances measured in the MF1 crystal structure. If the hyperfine interaction with ^{31}P is taken as axial with $A_{xx} = A_{yy} = a - F$ and $A_{zz} = a + 2F$, a is the isotropic part $a = A_{iso}$, and F is given by

$$F = \frac{g_e\beta_e g_N\beta_N}{hr^3}$$

where g_e is the electronic g value, and r the effective distance between the Mn and P atoms (*49*). In this manner, a and F can be estimated for $^{31}P_\beta$ of ADP bound to TF1, and for $^{31}P_\beta$ and $^{31}P_\gamma$ of AMP−PNP bound to TF1. The results are reported in Table 1. For Mn·TF1·ADP, $|A| =$ 5.20 MHz, the isotropic part is $a = 3.84$ MHz, and the anisotropic factor $F = 0.68$ MHz. It can be seen that the hyperfine coupling between the Mn^{2+} ion and the ligand ^{31}P is largely isotropic, with ~25% representing the anisotropic portion. The calculations performed above of the $|A(^{31}P)|$ based upon the separation of the ESEEM peaks in the 1D and 2D spectra were made provided that the anisotropic

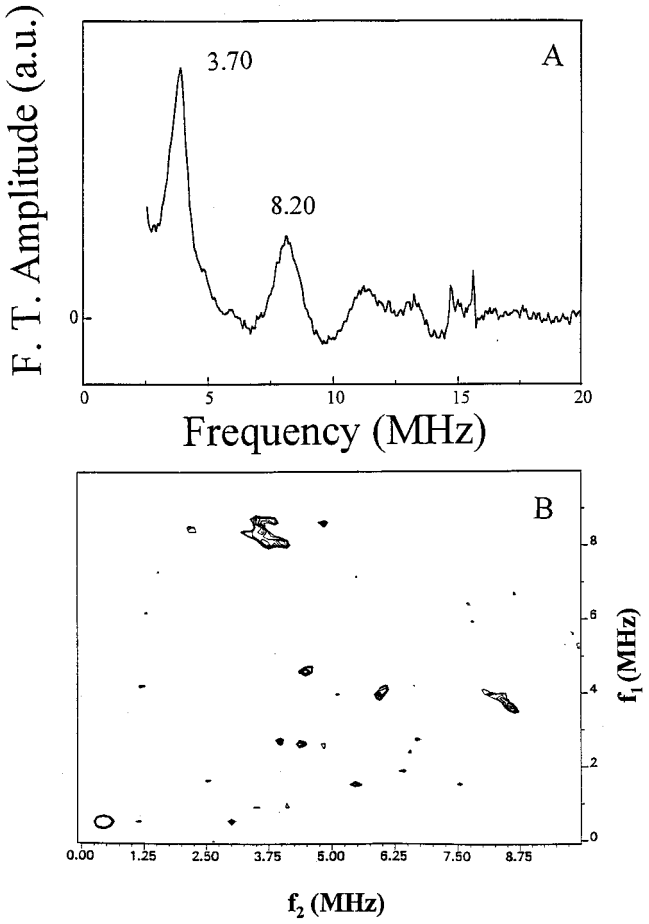

FIGURE 8: Three-pulse Fourier transform ESEEM spectra (A) and HYSCORE contour plot (B) of Mn^{2+} in the presence of the isolated β subunit and ATP (1 Mn/β and 1 ATP/β). The data were recorded with $\tau = 136$ ns, $H = 345.4$ mT, $f = 9.55$ GHz (A); and $\tau = 168$ ns, $H = 345.4$ mT, $f = 9.55$ GHz (B).

portion of the hyperfine coupling was small compared with the secular part. The present estimation of the anisotropic hyperfine terms actually supports this hypothesis. The data with AMP−PNP bound to TF1 are interpreted in a similar fashion (Table 1).

Interaction between the Isolated β Subunit and ATP. The nucleotide binding sites in F1 are located at the interfaces of the α and β subunits in the $\alpha_3\beta_3$ crown, and for the three catalytic sites, the residues involved in binding the nucleotides and the Mg^{2+} cations mainly originate from the β subunits (*2*, *3*, *50*). In an attempt to characterize the role of the α/β interfaces in providing the conformation of the active site that is required for ATP hydrolysis in TF1, the isolated β subunit was also studied by ESEEM and 2D HYSCORE spectroscopy in the presence of Mn^{2+} and ATP. Figure 8 shows the ESEEM and HYSCORE spectra obtained for a sample with Mn^{2+} and equimolar amounts of the β subunit and ATP. The spectrum displays two rather broad frequency components at 3.7 and 8.2 MHz, a pattern that resembles that obtained for the Mn^{2+} complexes with TF1 and AXP (Figure 1). The two ESEEM peaks at 3.7 and 8.2 MHz are therefore assigned to the hyperfine interaction with ^{31}P occurring through a Mn···Pi bond. It is of note that this ESEEM spectrum is quite similar to that obtained for the control ATP sample (Figure 4B). On the other hand, it has been reported that in the presence of divalent metal cations the β subunit is able to bind ATP, yet with a reduced affinity

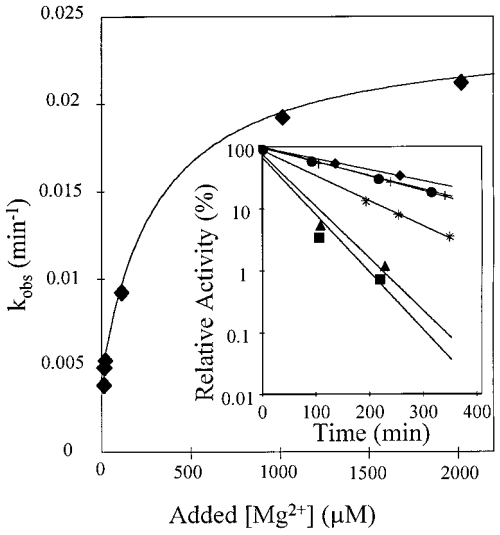

FIGURE 9: (Inset) Normalized TF1 activity vs time of incubation with fluoroaluminates. The enzyme (3.3 μM) was incubated at 60 °C with ADP (3.3 μM), $Al(NO_3)_3$ (200 μM), NaF (5 mM) and various concentrations of $MgCl_2$: no Mg^{2+} added (diamonds), 3.3 μM (circles), 10 μM (crosses), 100 μM (stars), 1 mM (triangles), 2 mM (squares). The ATPase activity of the enzyme at different times of incubation (t) was measured by following the absorbance change at 340 nm using the coupled enzymatic system pyruvate kinase and lactate dehydrogenase. The 100% value corresponds to a specific activity of 21 μmol ADP min^{-1} mg^{-1}. The inhibition profile follows a monoexponential progress $A_{340}(t) = A_0 \exp(-k_{obs}t)$ where A_0 is the initial absorbance of the reaction mixture and k_{obs} the experimental parameter. The main curve is the plot of the observed time constant of inhibition k_{obs} as a function of the added Mg^{2+} ion concentration. The observable constant k_{obs} of TF1 inhibition varies as a typical saturation function. The line drawn through the data is a hyperbolic function fit to the experimental data (see text).

compared with F1 (*6*). The present ESEEM data indicate that although most of the residues that build the catalytic site in TF1 originate from the β subunit, the isolated β subunit is not able to provide a fully active binding site for Mn·ATP. With $|A(^{31}P)| \approx 4.50$ MHz, the Mn·ATP complex with the β subunit has ESEEM properties undistinguishable from those in the absence of the β subunit, suggesting that the conformation of the ATP phosphate chain is similar to that in solution. This indicates that the isolated β subunit is not able to organize the conformation of the ATP nucleotide which is observed in fully active TF1. The presence of the α subunit is therefore important for maintaining a fully active nucleotide binding site in TF1 and for constraining the conformation of the nucleotide. The present ESEEM and HYSCORE data strongly support the view that in the absence of the α subunit the nucleotide binding site formed by the β subunit alone is partially structured, and therefore, the presence of the α subunit effectively participates in the formation of a fully active site.

Inhibition of TF1 Activity by Fluoroaluminates. The ATP hydrolysis reaction catalyzed by TF1 involves a transition state where the γ phosphate group is being cleaved. In an attempt to trap a complex of TF1 with a transition state analogue involving Mn^{2+} that could be studied by ESEEM and HYSCORE spectroscopy, we have investigated the effects of analogues of inorganic phosphate that mimic the transition state in enzymes that use triphosphate nucleosides during catalysis. It was found that 5 mM of orthovanadate (VO_4^{3-}), molybdate (MoO_4^{3-}) or tungstate (WO_4^{3-}) do not

inhibit the TF1 enzyme (3.3 μM) in the presence of ADP (3.3 μM) and Mg^{2+} (2 mM) at a temperature of 60 °C in time scales up to 5 h (data not shown). By contrast, fluoroaluminates (AlF_3 or AlF_4^-) appear to totally inhibit the enzyme. Figure 9 shows the inhibition profile of TF1 (3.3 μM) in the presence of 3.3 μM ADP, 200 μM $Al(NO_3)_3$ and 5 mM NaF with different concentrations of Mg^{2+}. This corresponds to a 60-fold excess of Al^{3+} and 1500-fold excess of F^- relative to the enzyme. For all the Mg^{2+} concentrations that were studied, the kinetics of the inhibition follows a monoexponential progress in the time scale from 200 up to 500 min (Figure 9, inset). It is of note that a small inhibition is observed even when Mg^{2+} is not added to the incubation medium. This effect may be assigned to the presence of residual Mg^{2+} that could remain tightly bound to TF1 or alternatively, of Mg^{2+} introduced as a minor contaminant in the buffers and reactants used. In both cases, this residual Mg^{2+} probably participates in the formation of the inhibited complex.

As shown in Figure 9, the observed time constant of inhibition, k_{obs}, varies as a hyperbolic function versus the added Mg^{2+} concentration. The data are compatible with the following kinetic model (*51*):

$$E + Mg^{2+} + ADP + AlF_x \overset{k_{-1}k_{+1}}{\longleftrightarrow} [E{\cdot}Mg{\cdot}ADP{\cdot}AlF_x] \overset{k_{-1}k_{+1}}{\longleftrightarrow} [E{\cdot}Mg{\cdot}ADP{\cdot}AlF_x]^* \quad \text{(Reaction I)}$$

where the second step corresponding to the isomerization of the complexed enzyme is the limiting step of the reaction. By contrast, the first step is fast and is only limited by the molecular diffusion rate constant. Under these conditions,

$$k_{obs} = k_{+2}\frac{[Mg^{2+}]}{(K_D + [Mg^{2+}])} \qquad \text{eq 2}$$

where k_{+2} is the isomerization rate constant and $K_D = k_{-1}/k_{+1}$ is the equilibrium dissociation constant of the [E·Mg·ADP·AlF_x] complex. [E·Mg·ADP·AlF_x]* is the isomerized complex which is the stable inhibited enzyme complex.

At high concentrations of Mg^{2+}, the k_{obs} value saturates at $k_{+2} \approx 0.02$ min^{-1}. The rather low value of k_{+2} will be discussed below. k_{-2} obtained as the intercept of the k_{obs} curve with the *y*-axis is very low compared with k_{+2}, and therefore it is neglected in the model. This confirms the high stability of the inhibited enzyme complex. The equilibrium dissociation constant $K_D = 350$ μM can be extracted from the fit. Its particularly high value will also be discussed below.

In the presence of a large excess of Al^{3+} and F^-, the ATPase activity of TF1 is inhibited, even when ADP and Mg^{2+} are present in concentrations that are stoichiometric with the enzyme concentration (Figure 9, inset, full circles). These experimental conditions, in particular the concentration of the metal cation with respect to the enzyme, are a prerequisite to the study of a complex suitable for EPR and ESEEM investigations. It is then possible to address the EPR spectroscopic characterization of one active site of the enzyme which is trapped in a potent transition state that contains Mn^{2+}. In a preliminary study it has been verified

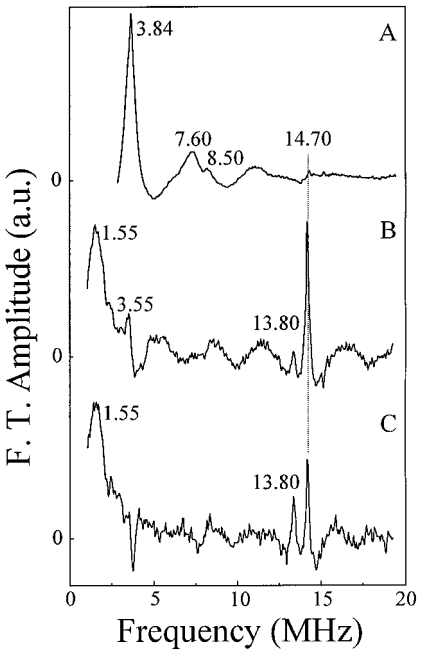

FIGURE 10: Three-pulse Fourier transform ESEEM spectra of Mn^{2+} (50 μM) bound to TF1 in stoichiometric conditions with added ADP (50 μM), $Al(NO_3)_3$ (3 mM), and NaF (75 mM). The sample was frozen after 6 h incubation at 60 °C corresponding to a maximum (99%) inhibition of TF1 activity. The data were recorded with T = 4.2 K, $f = 9.62$ GHz, with a magnetic field $H = 345.4$ mT. The interpulse time τ used in the pulse sequence was $\tau = 136$ ns (A), $\tau = 240$ ns (B), and $\tau = 256$ ns (C). The time interval between successive spin−echo pulse sets was 2 ms.

that the replacement of Mg^{2+} for Mn^{2+} yields similar inhibition results under identical conditions of reactant concentrations (not shown).

The putative formation of a transition state analogue involving Mn^{2+}, ADP, and AlF_x is interesting, because in view of the ESEEM and HYSCORE characterizations of the Mn·TF1·AXP complexes described above, it might be expected that superhyperfine couplings between the central Mn^{2+} ion and the fluorine ^{19}F ($I = {}^1/_2$) and/or aluminum ^{27}Al ($I = 5/2$) may be detected by EPR spectroscopy. Figure 10 shows a set of three-pulse ESEEM spectra of a sample of Mg^{2+}-depleted TF1 (50 μM) in the presence of Mn^{2+} (1 Mn/TF1) with added ADP (50 μM), $Al(NO_3)_3$ (3 mM), and NaF (75 mM). The sample examined here was frozen after an incubation period of 6 h at 60 °C corresponding to a maximum (99%) inhibition of enzyme activity. The three spectra that are shown were obtained with different values of the τ parameter, enabling different features to be highlighted in the ESEEM. Spectrum A was recorded with $\tau =$ 136 ns which, at the magnetic field $H = 345.4$ mT, virtually eliminates the contribution of the ^1H Larmor frequency to the ESEEM. The main nuclear frequency that is observed under these conditions (3.84 MHz) appears to closely match the ^{27}Al Larmor frequency, and was observed to vary accordingly when the external magnetic field was changed (not shown). It is of note, however, that due to the large excess of Na^+ ions in the sample (75 mM) and the close proximity of the ^{23}Na Larmor frequency (3.89 MHz at 345.4 mT), ^{23}Na dipolar couplings also certainly contribute to the ESEEM. The positive peak at 7.60 MHz is a combination line of the intense 3.84 MHz peak. Although much less intense and present only as a small feature on the rolling

baseline, the peak at 8.50 MHz in Figure 10A is a reproducible feature of the spectrum (see spectra B and C). It is tentatively assigned to a ^{31}P transition frequency based on both its magnetic field dependence and the comparison with the results shown in Figure 1. The Larmor frequency of the ^{19}F atom is $\nu_L = 13.84$ MHz at $H = 345.4$ mT, and this frequency might also be affected by the suppression effect due to the choice of $\tau = 136$ ns in spectrum A. Therefore, the ESEEM of the same inhibited sample was recorded with other τ values. Spectra B and C in Figure 10 are two representative ESEEM spectra obtained with $\tau = 240$ ns and $\tau = 256$ ns, respectively. At these τ values, the ESEEM frequencies in the 3.8 MHz region are expected to be largely suppressed, and this was indeed found in the experimental spectra with the nearly complete disappearance of the 3.84 MHz peak (Figure 9, panels B and C). By contrast, the Larmor frequency of ^1H develops at 14.70 MHz, together with a smaller component at 13.80 MHz that we assign to the Larmor frequency of ^{19}F nuclei. This demonstrates that the Mn^{2+} cation experiences coupling with ^{19}F atoms. The observation that the hyperfine coupling is manifest as an ESEEM peak centered at the ^{19}F Larmor frequency indicates that the hyperfine interaction is mainly dipolar and therefore essentially anisotropic. No other frequency component that could be assigned to ^{19}F was detected in the ESEEM. The peak at 3.55 MHz in spectrum B may be assigned to the low-frequency component of coupled ^{31}P.

Because it was shown in the previous section that under the experimental conditions used, the TF1 enzyme was completely inhibited, and because the inhibition data could be interpreted in terms of the formation of a complex with the transition state analogue AlF_x, the ESEEM data are also interpreted in terms of a complex with Mn^{2+} that represents the inhibited enzyme, namely [Mn·TF1·ADP·AlF_x]*. The ESEEM frequency measured at 8.50 MHz in Figure 10A corresponds to the coupling between Mn^{2+} and a ^{31}P atom from ADP. A rough estimate of the hyperfine coupling can be made using eq 1, $|A(^{31}P)| \approx 5.10$ MHz. This value is similar to but significantly smaller than that measured in the noninhibited enzyme in the absence of $Al(NO_3)_3$ and NaF, i.e., in the Mn·TF1·ADP complex ($|A(^{31}P)| \approx 5.20$ MHz, Table 1). This is interpreted as perturbation of the interaction between Mn and ADP upon formation of the complex with the transition state analogue, with probably an increased Mn···Pi bond length in the latter (see below). The detection of ^{19}F and probably also ^{27}Al ESEEM features at 13.80 and 3.84 MHz, i.e., at their respective Larmor frequencies indicates that in the inhibited complex the distances between the central Mn^{2+} ion and Al and F from AlF_x are smaller than 6 Å.

DISCUSSION

In the absence of nucleotide, TF1 binds Mn^{2+} ions. The ESEEM spectrum of a stoichiometric complex Mn·TF1 indicates that at least one of the ligands of the Mn^{2+} ion cofactor is a ^{14}N atom. It was argued in a previous study that the deprotonated ϵ amine of β-Lys-164 which is located at a nucleotide binding site could be the ligand of the bound Mn^{2+} (*24*). Relevant to this interpretation, the examination of the crystal structure of the analogous MF1 (*2*) is informative. First, in the MF1 crystal, none of the three nucleotide binding sites β_{DP}, β_{TP}, and β_E is fully comparable to the situation examined here for TF1: the β_E site is empty and contains no metal cation, and the β_{DP} and β_{TP} sites are both filled with Mg^{2+} and a nucleotide. In the β_{DP} and β_{TP} sites, however, a number of peptide nitrogen atoms are in close proximity to the Mg^{2+} cation and may be believed to be involved in its binding when the nucleotide is absent. The first candidate is the N_α of β-Lys162 in MF1, which is located at distances from Mg^{2+} 5.80 Å in β_{TP} and 5.70 Å in β_{DP}. The ϵ amine nitrogen of β-Lys162 is also close at 5.36 Å (β_{TP}) and 5.20 Å (β_{DP}). The N_α of β-Thr163 (4.18 Å in β_{TP} and 4.09 Å in β_{DP}) and possibly of β-Val164 (6.05 Å in β_{TP} and 6.03 Å in β_{DP}) are alternative candidates. Interestingly, the guanidinium nitrogens of β-Arg189 appear also to be located at relatively small distances (3.97, 5.88, and 6.02 Å in β_{TP}; 4.08, 5.74, and 6.33 Å in β_{DP}) that are compatible with binding of the divalent metal when the nucleotide is absent. All these atoms are the closest nitrogen atoms to the Mg^{2+} that have been identified. Although the effective ionic radius of Mn^{2+} (0.83 Å) is slightly larger than Mg^{2+} (0.72 Å), it is reasonable to envision that in Mn^{2+} substituted TF1, the binding mode of the metal cation is close to that of Mg^{2+}. We propose that in the absence of nucleotide, one of the closest nitrogen atoms identified above is displaced and serves as a ligand to the metal cation.

For TF1 with Mn^{2+} and in the presence of nucleotide (ADP, ATP, or AMP−PNP), the ESEEM and HYSCORE data reported above demonstrate that the conformation of the nucleotide molecule, especially its phosphate chain is modified by the presence of the enzyme. More specifically, the data unambiguously show that the magnetic hyperfine interactions between the Mn^{2+} ion and the ^{31}P atoms from the phosphate chain in the active site are different from those measured in solution. In other words, the particular conformation of the nucleotide relative to the Mn^{2+} ion in TF1 gives rise to specific signatures in the EPR spectra, which are quantitated by the hyperfine coupling parameter $A(^{31}P)$ (Table 1). It has been mentioned above that due to the high spin multiplicity of Mn^{2+}, the hyperfine coupling interactions in Table 1 are only approximate, but it is the relative differences between the different samples examined in the present study that are especially informative here.

The hyperfine couplings include the isotropic part which is a measure of the electron spin density from the Mn^{2+} onto the ^{31}P nuclei. It is therefore highly dependent on the bonding properties between those two atoms. On the other hand, the anisotropic part is only dependent on the distance between the Mn and the P atoms. We have estimated these distances in the Mn·TF1·ADP and Mn·TF1·AMP−PNP complexes studied here using the distance measurements made from the MF1 crystal structure. The relevant distances are measured in the β_{DP} site filled with ADP where the Mg^{2+} is coordinated by the β phosphate resulting in a $Mg\cdots P_\beta$ distance of 3.607 Å. The anisotropic factor $F = 0.68$ MHz can be estimated from the point dipole model (Table 1). Since the α phosphorus atom is at 4.866 Å from the Mg^{2+}, and the nearest O_α is at 4.705 Å, the α phosphate cannot bind the Mg^{2+} and therefore does not contribute to the observed hyperfine coupling. It is concluded that $|A(^{31}P)| \approx 5.20$ MHz corresponds to the β phosphate with the coordinating oxygen at 2.285 Å. This in turn yields an estimated isotropic hyperfine coupling of 3.84 MHz for this interaction. In the

β_{TP} site, the distances between the three phosphorus atoms P_γ, P_β and P_α and the Mg^{2+} are 3.529, 3.699, and 5.107 Å respectively. The estimations for the anisotropic parts *F* of the corresponding hyperfine interactions are 0.73, 0.63, and 0.24 MHz, respectively. However, the distances between the Mg^{2+} and the O_α are incompatible with binding of the Mn^{2+} by the α phosphate ($d > 4.44$ Å). For the P_β and P_γ, the Mg···O···P bonding scheme shows that the Mg···O distance is longer (2.439 Å) for the P_β than for the P_γ (2.197 Å), whereas the O···P distances are similar (1.524 and 1.506 Å), and the Mg−O−P angle is closer to the straight angle for P_γ than for P_β. This situation is likely to convey a smaller isotropic hyperfine coupling for P_β. Therefore, it is concluded that in TF1 with AMP−PNP the $^{31}P_\beta$ and $^{31}P_\gamma$ from the two phosphate ligands yield $|A(^{31}P_\beta)| \approx 4.20$ MHz and $|A(^{31}P_\gamma)| \approx 5.40$ MHz, respectively. By analogy and for the spectroscopic results with ATP, it is concluded that in the active site, Mn^{2+} is bound through the two terminal phosphates of ATP with $|A(^{31}P_\beta)| \approx 4.60$ MHz and $|A(^{31}P_\gamma)| \approx 5.90$ MHz. Interestingly, it is found that the hyperfine couplings with $^{31}P_\beta$ and $^{31}P_\gamma$ are larger for ATP than for AMP−PNP. Because the ATP and AMP−PNP molecules and their binding with metal cations are analogous, and because it seems reasonable, in the present situation, to consider that an increase in the $|A(^{31}P)|$ parameter corresponds to a decrease in the corresponding Mg···O bond, it is suggested that the Mn···O_β and Mn···O_γ distances are smaller for ATP than for AMP−PNP.

The ESEEM and HYSCORE spectra of Mn^{2+} bound to TF1 and triphosphate nucleosides are interpreted above in terms of two ^{31}P hyperfine couplings being resolved. This seems reasonable by comparison of the ESEEM and HYSCORE spectra measured for TF1 in the presence of diphosphate nucleosides, which provide a single phosphate ligand to the Mn^{2+}. It is of note, however, that the ESEEM of the systems studied here is relatively weak, suggesting that only one ^{31}P from the triphosphate ligand may contribute to the ESEEM. In this alternative interpretation, the complex line shapes observed in the HYSCORE of the Mn·TF1·ATP and Mn·TF1·AMP−PNP may therefore reflect the anisotropy of the hyperfine interaction. Compatible with this idea, the length of the oblong contours of the HYSCORE is in the 1.5−2.0 MHz range, which is close to the 3**F* value, the anisotropic portion of the axial tensor calculated with the point dipole approximation (Table 1). This alternative interpretation would therefore emphasize the increased anisotropy of the resolved ^{31}P hyperfine interaction for the bound triphosphate nucleosides compared with the analogous diphosphates.

For the isolated β subunit in the presence of Mn^{2+} and ATP, the ESEEM data indicate a hyperfine coupling $|A(^{31}P)| = 4.50$ MHz, i.e., similar to that measured for the control Mn·ATP complex in the absence of protein. Although it has been reported that the isolated β subunit binds nucleotides in the presence of divalent metal cations, the stoichiometric conditions used here for the ESEEM measurements are probably not adequate to promote the formation of the ternary complex Mn·β·ATP. Alternatively, Mn^{2+} and ATP may bind to the isolated β subunit, but with no change in the arrangement of the triphosphate chain and its interaction with Mn^{2+}, as opposed to what is observed with full TF1.

The TF1 enzyme has been trapped in a transition state analogue using fluoroaluminate anions as analogues of the inorganic phosphate. The successful formation of the transition state using stoichiometric TF1, Mn^{2+}, and ADP concentrations is in line with the finding that the formation of the transition state analogue at a single catalytic site is sufficient for complete inhibition of the wild type $\alpha_3\beta_3\gamma$ subcomplex of TF1 (*19*). Further, the kinetics of the inhibition indicates that with stoichiometric concentrations of Mg^{2+} and ADP, TF1 is completely inactivated after 6 h of incubation with an excess of Al^{3+} and F^-. The data indicate that for this experiment Mg^{2+} can easily be replaced for Mn^{2+}, and that very similar inhibition results are obtained (not shown). In fact, the rate of inhibition with Mn^{2+} is slightly higher than with Mg^{2+}, and this effect is assigned to the higher affinity of Mn^{2+} for ADP than Mg^{2+}, the Me^{2+}·ADP complex being the active ligand form.

The kinetic data reported here are compatible with the model outlined by reaction I. The bimolecular step is expected to be fast and is not directly observable in the kinetics. The rate of the single step should be modeled by eq 2 (*51*). According to this model, the observed rate (k_{obs}) should increase with the concentration of Mg^{2+} and reach a plateau value equal to k_{+2}, the true rate of TF1 isomerization after binding of ADP, Mg^{2+}, and AlF_x, with a half saturation occurring for $[Mg^{2+}] = k_{-1}/k_{+1} = K_D$, the equilibrium dissociation constant of the inhibited complex. The backward reaction of dissociation of the isomerized inhibited enzyme complex is very slow and its rate k_{-2} can be neglected. The experimental data were fitted to eq 2 (Figure 9) and yield a rate constant $k_{+2} = 0.02$ min^{-1} and a dissociation constant $K_D = 350$ μM. The relatively low value of the rate constant of isomerization, k_{+2}, is due to the experimental conditions used, especially the stoichiometric concentration of ADP. In the presence of an excess of ADP, the inhibition rate constant is increased (not shown). When the overall protein conformation is modified as for the $\alpha_3\beta_3\gamma$ subcomplex of TF1, the rate constant of isomerization measured under similar experimental conditions is lowered by a factor of 3 (*19*). Further, the measured K_D is relatively high (350 μM), indicating that the affinity of AlF_x for the TF1·ADP complex is rather low, which seems rather surprising. In fact, quite analogous results have been reported with the UMP kinase from *Dictyostelium discoideum* (*52*). In this latter case, the low affinity for AlF_x was explained by the fact that the ADP·AlF_x complex was not a covalent transition-state analogue, this situation generating an unfavorable entropic factor. Furthermore, in solution and at neutral pH, the dominant complex formed after mixing $AlCl_3$ and NaF in the presence of ADP is ADP·AlF_4−OH (*53*). Therefore, AlF_3 appears to be a minor species in solution. Based on these considerations, the low affinity of AlF_x for TF1 may be a strong indication that TF1 binds only the trivalent AlF_3, which is not abundant in solution, and not the tetravalent AlF_4^-. This in turn could also explain why it was found that TF1 binds neither vanadate (VO_4^{3-}), molybdate (MoO_4^{3-}), nor tungstate (WO_4^{3-}), which are also tetravalent. Only two enzymes have been described as binding AlF_3, namely the NDP kinase (*18*) and the UMP kinase (*52*) from *Dictyostelium*, and in the crystal structures of the G proteins $G_{t\alpha}$ and $G_{i\alpha}$, the presence of the AlF_4−OH moiety probably reflects the fact that the active sites are too weak to enforce the binding of AlF_3 (*54*,

55). In other words, the protein residues in the active site of TF1 and the ADP nucleotide may build a constrained environment and therefore it is likely that the complex with AlF_3 closely mimics the protein and substrate geometries in the transition state. The plasticity of the protein active site that was inferred from the observation of complexes of myosin, Mg·ADP, and octahedral AlF_4^- or trigonal vanadate (*56*) is much smaller in the active site of TF1 and does not accommodate the binding of AlF_4^-. It has however been reported that this steric hindrance for AlF_4^- and for vanadate depends on the nature of the nucleophilic attack, which involves a protein group instead a water molecule (*18*). Our results seem therefore to indicate that even when a water molecule is the acceptor in the phosphoryl transfer, AlF_3 may be the bound entity at the active site with the geometry of the transition state. In this respect, the inhibition results of MF1 from rat liver in the presence of VO_4^{3-} (*25*) may be taken as an illustration of different active site plasticities for H^+-ATPases from two different phylogenic organisms. However, it is of note that VO_4^{3-}, like AlF_4^-, is not a true analogue for the transition state of phosphate, and it is possible that MF1 may rearrange around the vanadate in a conformation that is not a true transition state.

The ESEEM data of the inhibited enzyme complex with Mn^{2+}, ADP, and AlF_3 indicate that the interaction between the Mn^{2+} and the β phosphate of ADP is modified compared with that in Mn·TF1·ADP. Although it is difficult to obtain an accurate measurement of the hyperfine interaction due to the presence of other broad peaks in the same frequency region, the position of the ^{31}P ESEEM peak (~8.50 MHz) suggests that the ^{31}P hyperfine coupling and probably the $Mn\cdots O_\beta$ distance in the complex with the transition-state analogue is intermediate between those with ADP and ATP.

The observation of a ^{19}F modulation at 13.80 MHz in the stimulated ESEEM, i.e., only at the Larmor frequency ν_L of ^{19}F indicates that the interaction between Mn^{2+} and the ^{19}F nuclei takes place in the weak coupling limit. There is no evidence for an isotropic hyperfine interaction of significant magnitude as would be expected if the fluorine atoms from the AlF_3 were directly coordinated to the Mn^{2+}. Also, we have not found any description of a complex of Mn^{2+} with fluoride ligands in the literature, perhaps due to the oxidation of Mn^{2+} to Mn^{3+}. This also indicates that the distance between the Mn^{2+} and the ^{19}F atoms is at least 2.85 Å (*48*). In addition, it has been shown that the lower limit for detection of low abundant ^{13}C and ^{15}N ESEEM weakly coupled to Mn^{2+} bound to p21 *ras* corresponded to a maximum distance of 6 Å (*42*). On this basis, it is concluded that the detection of the modulation of weakly coupled ^{19}F in the inhibited complex Mn·TF1·ADP·AlF_3 that is studied here also reflects the presence of ^{19}F atoms at distances lower than 6 Å from the Mn^{2+}. In fact, classical methods for extracting the number and distance of nuclei with weak hyperfine interaction require the measurement of both the fundamental ν_L and harmonic $2\nu_L$ frequencies that are present in the primary ESEEM modulation function. As mentioned above, not only ^{19}F atoms, but also ^1H, ^{23}Na and possibly ^{27}Al frequencies contribute to the ESEEM, and the ^{19}F modulation frequencies can only be detected with adequate use of the suppression effect, i.e., in the stimulated ESEEM. Therefore it is presently difficult to extract more precise information on the number and distances of the AlF_3 fluorine atoms from the ESEEM data.

ACKNOWLEDGMENT

We thank Dr. Stéphane Esnouf, DRECAM/SRSIM, CEA/Saclay for recording the EPR spectra at Q-band. We also thank Mr. Nicolas Sanchez and Ms. Gwénaëlle Moal for skillful help in the preparation of TF1 and Dr. Francis Haraux for useful discussions. This work was performed while B.S. was Scientifique du Contingent at CEA as fulfillment of the Service National.

REFERENCES

1. Weber, J., and Senior, A. E. (1997) *Biochim. Biophys. Acta 1319*, 19−58.
2. Abrahams, J. P., Leslie, A. G. W., Lutter, R., and Walker, J. E. (1994) *Nature 370*, 621−628.
3. Shirakihara, Y., Leslie, A. G. W., Abrahams, J. P., Walker, J. E., Ueda, T., Sekimoto, Y., Kambara, M., Saika, K., Kagawa, Y., and Yoshida, M. (1997) *Structure 5*, 825−836.
4. Cross, R. L., and Nalin, C. M. (1992) *J. Biol. Chem. 257*, 2874−2881.
5. Wise, J. G., Duncan, T. M., Latchney, L. R., Cox, D. N., and Senior, A. E. (1983) *Biochem. J. 215*, 343−350.
6. Girault, G., Berger, G., Galmiche, J.-M., and André, F. (1988) *J. Biol. Chem. 263*, 14690−14695.
7. Cross, R. L. (1988) *J. Bioenerg. Biomembr. 20*, 395−406.
8. Senior, A. E. (1990) *Annu. Rev. Biophys. Biophys. Chem. 19*, 7−41.
9. Senior, A. E., Wilke-Mounts, S., and Al-Shawi, M. K. (1993) *J. Biol. Chem. 268*, 6989−6994.
10. Fersht, A. R. (1985) in *Enzyme Structure and Mechanism* (Freeman, W. H., Ed.), pp 235−243, New York.
11. Webb, M. R., Grubmeyer, C., Penefsky, H. S., and Trentham, D. R. (1980) *J. Biol. Chem. 255*, 11637−11639.
12. Senter, P., Eckstein, F., and Kagawa, Y. (1983) *Biochemistry 22*, 5514−5518.
13. Bigay, J., Deterre, P., Pfister, C., and Chabre, M. (1987) *EMBO J. 6*, 2907−2913.
14. Carlier, M. F., and Pantaloni, D. (1993) *Handbook of Experimental Pharmacology*, Vol. 108/I, pp 53−62, Springer-Verlag, Berlin.
15. Combeau, C., and Carlier, M. F. (1988) *J. Biol. Chem. 263*, 17429−17436.
16. Issartel, J. P., Dupuy, A., Lunardi, J., and Vignais, P. (1991) *Biochemistry 30*, 4726−4733.
17. Mittal, R., Ahmadian, M. R., Goody, R., and Wittinghofer, A. (1996) *Science 273*, 115−117.
18. Xu, Y. W., Moréra, S., Janin, J., and Cherfils, J. (1997) *Proc. Natl. Acad. Sci. U.S.A.* 94, 3579−3583.
19. Dou, C., Grodsky, N. B., Matsui, T., Yoshida, M., and Allison, W. S. (1997) *Biochemistry 36*, 3719−3727.
20. Hochman, Y., and Carmeli, C. (1981) *Biochemistry 20*, 6287−6292.
21. Weber, J., Wilke-Mounts, S., and Senior, A. E. (1994) *J. Biol. Chem. 269*, 20462−20467.
22. Weber, J., and Senior, A. E. (1996) *J. Biol. Chem. 271*, 3474−3477.
23. Hiller, R., and Carmeli, C. (1985) *J. Biol. Chem. 260*, 1614−1617.
24. Buy, C., Girault, G., and Zimmermann, J.-L. (1996) *Biochemistry 35*, 9880−9891.
25. Ko, Y. H., Bianchet, M., Amzel, L. M., and Pedersen, P. L. (1997) *J. Biol. Chem. 272*, 18875−18881.
26. Ohta, S., Tsuboi, M., Oshima, T., Yoshida, M., and Kagawa, Y. (1980) *J. Biochem. 87*, 1609−1617.
27. Ohta, S., Yohda, M., Ishizuka, M., Hirata, H., Hamamoto, T., Otawara-Hamamoto, Y., Matsuda, K., and Kagawa, Y. (1988) *Biochim. Biophys. Acta 933*, 141−155.
28. Tozawa, K., Odaka, M., Date, T., and Yoshida, M. (1992) *J. Biol. Chem. 267*, 16484−16490.

29. Jault, J.-M., and Allison, W. S. (1994) *J. Biol. Chem. 269*, 319−325.
30. Markham, G. D., Nageswara, Rao, B. D., and Reed, G. H. (1979) *J. Magn. Reson. 33*, 4486−4491.
31. Reed, G. H., and Markham, G. D. (1984) in *Biological Magnetic Resonance* (Berliner, L. J., and Reuben, J., Eds.) Vol. 6, pp 73−142, Plenum Press, New York.
32. Fauth, J. M., Schweiger, A., Braunschweiler, L., Forrer, J., and Ernst, R. R. (1986) *J. Magn. Reson. 66*, 74−85.
33. Höfer, P., Grupp, A., Nebenführ, H., and Mehring, M. (1986) *Chem. Phys. Lett. 132*, 279−282.
34. Gemperle, C., Aebli, G., Schweiger, A., and Ernst, R. R. (1990) *J. Magn. Reson. 88*, 241−256.
35. Höfer, P. (1991) in *Electron Magnetic Resonance of Disordered Systems* (Yordanov, N. D., Ed.) pp 1−15, World Scientific, Singapore.
36. Buy, C., Matsui, T., Andrianambinintsoa, S., Sigalat, C., Girault, G., and Zimmermann, J.-L. (1996) *Biochemistry 35*, 14281−14293.
37. Shimizu, T., Mims, W. B., Davis, J. L., and Peisach, J. (1983) *Biochim. Biophys. Acta 757*, 29−39.
38. LoBrutto, R., Smithers, G. W., Reed, G. H., Orme-Johnson, W. H., Tan, S. L., and Leigh, J. S., Jr. (1986) *Biochemistry 25*, 5654−5660.
39. Eads, C. D., LoBrutto, R., Kumar, A., and Villafranca, J. J. (1988) *Biochemistry 27*, 165−170.
40. Tipton, P. A., McCracken, J., Cornelius, J. B., and Peisach, J. (1989) *Biochemistry 28*, 5720−5728.
41. Larsen, R. G., Halkides, C. J., and Singel, D. J. (1993) *J. Chem. Phys. 98*, 6704−6721.
42. Farrar, C. T., Halkides, C. J., and Singel, D. J. (1997) *Structure 5*, 1055−1066.
43. Senior, A. E., and Al-Shawi, M. K. (1992) *J. Biol. Chem. 269*, 20462−20467.
44. Löbau, S., Weber, J., Wilker-Mounts, S., and Senior, A. E. (1997) *J. Biol. Chem. 272*, 3648−3656.
45. Dikanov, S. A., and Bowman, M. K. (1995) *J. Magn. Reson. A 116*, 125−128.
46. Reijerse, E. J., Shane, J., de Boer, E., Höfer, P., and Collison, D. (1991) in *Electron Magnetic Resonance of Disordered Systems* (Yordanov, N. D., Ed.) pp 253−271, World Scientific, Singapore.
47. Shane, J. J., Höfer, P., Reijerse, E. J., and de Boer, E. (1992) *J. Magn. Reson. 99*, 596−604.
48. Dikanov, S. A., and Tsvetkov, Y. D. (1992) *Electron Spin−Echo Envelope Modulation (ESEEM) Spectroscopy*, CRC Press, Boca Raton, FL.
49. Chien, J. C. W., and Dickinson, L. C. (1981) in *Biological Magnetic Resonance* (Berliner, L. J., and Reuben, J., Eds.) Vol. 3, pp 155−211, Plenum Press, New York.
50. Weber, J., Hammond, S. T., Wilke-Mounts, S., and Senior, A. E. (1998) *Biochemistry 37*, 608−614.
51. Bernasconi, C. F. (1976) *Relaxation Kinetics*, pp 20−39, Acad. Press, New York.
52. Schlichting, I., and Reinstein, J. (1997) *Biochemistry 36*, 9290−9296.
53. Martin, R. B. (1996) *Coord. Chem. Rev. 149*, 23−32.
54. Coleman, D. E., Berghuis, A. M., Lee, E., Linder, M. E., Gilman, A. G., and Sprang, S. R. (1994) *Science 265*, 1405−1412.
55. Sondek, J., Lambright, D. G., Noel, J. P., Hamm, H. E., and Sigler, P. B. (1994) *Nature 372*, 276−279.
56. Smith, C. A., and Rayment, I. (1996) *Biochemistry 35*, 5404−5417.

BI0014599